

# XUV ionization of the H<sub>2</sub> molecule studied with attosecond angular streaking

Vladislav V. Serov<sup>1</sup> and Anatoli S. Kheifets<sup>2</sup>

<sup>1</sup>*General, Theoretical and Computer Physics, Saratov State University, Saratov 410012, Russia and*

<sup>2</sup>*Research School of Physics, The Australian National University, Canberra ACT 2601, Australia\**

(Dated: August 24, 2022)

We study orientation and two-center interference effects in attosecond time-resolved photoionization of the H<sub>2</sub> molecule. Time resolution of XUV ionization of H<sub>2</sub> is gained through the phase retrieval capability of attosecond angular streaking demonstrated earlier by Kheifets *et al* [arXiv:2202.06147 (2022)]. Once applied to H<sub>2</sub>, this technique delivers an anisotropic phase and time delay which both depend sensitively on the molecular axis orientation. In addition, the photoelectron momentum distribution displays a very clear two-center interference pattern. When the interference formula due to Walter and Briggs [J. Phys. B **32** 2487 (1999)] is applied, an effective photoelectron momentum appears to be greater than the asymptotic momentum at the detector. This effect is explained by a molecular potential well surrounding the photoemission center.

PACS numbers: 32.80.Rm 32.80.Fb 42.50.Hz

Attosecond time resolved studies of molecular photoionization have become a rapidly growing field. Starting from the pioneering experiment of Huppert *et al.* [1] on H<sub>2</sub>O and N<sub>2</sub>O, the method of attosecond interferometry has been progressively used combining an extreme-ultraviolet (XUV) attosecond pulse train (APT) and a synchronized infrared (IR) pulse. This technique has also been known as reconstruction of attosecond beating by interference of two-photon transitions (RABBITT) [2, 3]. Recent applications of RABBITT to molecular photoionization include attosecond resolution of coupled electron and nuclear dynamics in dissociative ionization of H<sub>2</sub> [4] and orientation-dependent time delay and electron localization studies in CO [5]. Nandi *et al.* [6] resolved attosecond timing of electron emission from a shape resonance in N<sub>2</sub>. Kamalov *et al.* [7] recorded electron correlation effects in attosecond photoionization of CO<sub>2</sub>. Wang *et al.* [8] explored the role of nuclear-electronic coupling in attosecond photoionization of H<sub>2</sub>.

The roadmap of atomic and molecular physics [9] has identified X-ray free-electron lasers (XFELs) as a promising tool for resolving ultrafast molecular dynamics. Attosecond time-energy structure of XFEL pulses has been recently demonstrated [10, 11]. This demonstration makes XFEL sources potentially suitable for attosecond time resolution of atomic and molecular photoionization. The only stumbling block preventing such an application is a stochastic nature and an inherent time jitter of XFEL radiation.

The method of attosecond angular streaking of XUV ionization was developed to overcome this obstacle. Prompted by theoretical works [12–15], this method was eventually implemented in practice for a shot-to-shot characterization of isolated attosecond pulses (IAP) at XFEL [10, 11]. Angular streaking of XUV ionization (ASXUVI or ASX for brevity) has common elements with

the two previously developed techniques: attosecond angular streaking known as the attoclock [16–18] and the attosecond streak camera (ASC) [19–26]. As in ASC, ASX uses XUV pulses to ionize the target. Then, similarly to the attoclock, the photoelectrons are steered by a circularly polarized laser field which makes its imprint on the photoelectron momentum distribution (PMD). This imprint is most visible in the plane perpendicular to the laser propagation direction. In its original form [10, 11, 13–15], ASX employed an intense IR laser field and was interpreted within the strong field approximation (SFA) [27]. In these strong field settings, the phase of the XUV ionization is usually neglected and the timing information associated with this phase is lost. An alternative view within the lowest order perturbation theory (LOPT) [28–30] considers IR streaking as an interference phenomenon which opens a natural access to the streaking phase  $\Phi_S$ . The latter is typically decomposed into the XUV ionization phase (or Wigner phase) and the continuum-continuum (CC) phase from the IR interaction. These two phases can be converted to the corresponding time delay components, which add up to the atomic time delay  $\tau_a$ .

Phase retrieval capability of ASX based on this analysis was demonstrated recently by Kheifets *et al.* [31]. In their numerical simulations on the hydrogen atom, they recovered accurately the streaking phase and the atomic time delay across a wide range of photon energies starting from the threshold and exceeding it many times. Most importantly, this phase retrieval could be conducted from a single XUV shot. This is a significant advantage over the existing interferometric techniques which require a systematic and controllable variation of the XUV/IR pulse delay in one set of measurements in order to record a streaking spectrogram or a RABBITT trace. This recording requires a precise and stable temporal synchronization of the XUV/IR pulses which is not feasible at XFEL at present.

In this paper, we extend ASX to molecular photoionization. We solve numerically the time-dependent

---

\*Electronic address: A.Kheifets@anu.edu.au

Schrödinger equation (TDSE) describing the hydrogen molecule driven by a combination of the linearly polarized XUV and circularly polarized IR pulses. In our simulations, the XUV/IR pulse delay is incremented in several steps. By augmenting the isochrone analysis proposed by Kazansky et al. [13] with the energy dependent XUV ionization phase, we are able to interpret the molecular TDSE results in terms of the atomic time delay. While the phase and time delay determination is most accurate combining several increments of the XUV/IR delay, the accuracy is not significantly compromised with just a single XUV/IR pulse delay. We make a comparison with the previous RABBITT simulations on  $\text{H}_2$  [32] and confirm validity of our interpretation and accuracy of our numerical results. We also demonstrate a strong dependence of the time delay on the molecular axis orientation discovered earlier in  $\text{H}_2^+$  ion [33, 34].

The paper is organized into the following sections. In Sec. I we outline basics of the ASX method. In Sec. II we describe our computational procedure. In Sec. III we analyze and interpret our numerical results. In Sec. IV we give our concluding remarks.

## I. BASIC CONSIDERATIONS

The proposed phase retrieval by ASX is outlined in our preceding work [31]. The basics of the molecular ASX are essentially the same as for atoms. We proceed as follows. We apply the SFA and write the photoionization amplitude as [35]

$$a(\mathbf{k}, \tau) = i \int_{t_0}^{\infty} dt E_x(t - \tau) D_x[\mathbf{k} - \mathbf{A}(t)] e^{-i\Phi(t)}. \quad (1)$$

Here the electric field of the XUV pulse  $E_x$  is advancing the streaking pulse by the time  $\tau$ . The streaking field is described by its vector potential

$$\mathbf{A}(t) = A_0 \cos(\omega t) \hat{\mathbf{x}} + A_0 \sin(\omega t) \hat{\mathbf{y}}.$$

The photoelectron momentum is confined to the polarization plane  $\mathbf{k} = k \cos \phi \hat{\mathbf{x}} + k \sin \phi \hat{\mathbf{y}}$ , where  $\phi$  is the emission angle.

The exponential term contains the phase factor

$$\Phi(t) = \frac{1}{2} \int_t^{\infty} dt' [\mathbf{k} - \mathbf{A}(t')]^2 - E_0 t, \quad (2)$$

which contains the photoelectron energy in the absence of streaking  $E_0 = \Omega - I_p$ . The most probable photoelectron trajectory, starting at the time  $t_{\text{st}}$ , keeps the phase stationary:

$$\Phi'(t_{\text{st}}) = \frac{1}{2} |\mathbf{k} - \mathbf{A}(t_{\text{st}})|^2 - E_0 = 0 \quad (3)$$

We assume that the XUV pulse is short relative to the IR pulse and shifted relative to its peak position by the

time  $\tau$ . Under these conditions, Eq. (3) is transformed to the following *isochrone* equation [13]:

$$k^2/2 - E_0 = k A_0 \cos(\phi - \omega\tau) \quad (4)$$

Here we neglect the ponderomotive energy  $U_p = A_0^2/2$  in a weak streaking field.

The above stationary phase analysis should be modified to account for the photoelectron energy dependence of the dipole matrix element [36]

$$\arg \{D[\mathbf{k} - \mathbf{A}(t)]\} \propto \alpha |\mathbf{k} - \mathbf{A}(t)|^2/2, \quad (5)$$

where

$$\alpha = \partial \arg D(\sqrt{2E})/\partial E \quad (6)$$

The modified stationary phase equation reads

$$\frac{1}{2} |\mathbf{k} - \mathbf{A}(t_{\text{st}})|^2 - E_0 + \frac{\alpha}{2} \frac{d}{dt} [(\mathbf{k} - \mathbf{A}(t_{\text{st}}))^2] = 0 \quad (7)$$

This leads to a generalized isochrone equation

$$\begin{aligned} k^2/2 - E_0 &= k A_0 [\cos(\phi - \omega\tau) - \alpha \omega \sin(\phi - \omega\tau)] \\ &\approx k A_0 \cos[\phi - \omega\tau + \omega\alpha] \end{aligned} \quad (8)$$

Here  $\alpha = \Phi_S/\omega = \tau_a$  under certain XUV and IR pulse parameters as demonstrated in [31].

## II. COMPUTATIONAL DETAILS

We solve numerically the molecular TDSE equation using the computer code [37] to obtain the ionization amplitude  $f(\mathbf{k})$ . We use an angular basis that included spherical harmonics up to  $l_{\text{max}} = 7$  and  $|m_{\text{max}}| = 7$ . Unlike the dipole selection rules in atomic XUV photoionization, the quantum numbers  $l, m$  adhere to the parity conservation.

The photoelectron momentum spectrum  $P(\mathbf{k})$  is obtained as the modulus squared of the ionization amplitude

$$P(\mathbf{k}) \propto |f(\mathbf{k})|^2. \quad (9)$$

The PMD is restricted to the polarization plane  $P(k_x, k_y, k_z = 0)$  and converted to the polar coordinates  $P(k, \phi)$  where

$$k = (k_x^2 + k_y^2)^{1/2}, \quad \phi = \tan^{-1}(k_y/k_x). \quad (10)$$

In these coordinates, we define the directional probability of the photoelectron emission

$$P(\phi) = \int dk P(k, \phi) \quad (11)$$

and the mean (central) radial momentum in the given direction

$$\bar{k}(\phi) = \int k P(k, \phi) dk / P(\phi). \quad (12)$$

The TDSE is driven by the XUV and IR pulses with the following parameters. The XUV pulse with a Gaussian envelope has a FWHM of 2 fs and the intensity of  $6 \times 10^{13}$  W/cm<sup>2</sup>. The XUV photon energy  $\Omega$  ranges from 0.7 au to 3 au. A relatively low XUV field intensity is required to remain within the LOPT framework. A fairly large pulse duration is employed to ensure a moderately narrow spectral width to probe XUV ionization sufficiently close to the threshold at 15.6 eV (0.57 au). At the same time, the spectral width  $\Gamma$  should be kept sufficiently large to make sure the IR assisted XUV absorption process overlaps spectrally with unassisted XUV ionization [31]. This requires  $\Gamma > 2\omega$ , where  $\omega$  is the laser photon energy. To satisfy this requirement, we chose a mid-IR laser pulse with  $\omega = 0.038$  au corresponding to  $\lambda = 1200$  nm. The pulse has a cosine squared envelope with FWHM of 25 fs and the intensity of  $1.5 \times 10^{11}$  W/cm<sup>2</sup>. The XUV pulse is linearly polarized along the  $\hat{x}$  axis whereas the IR pulse is circularly polarized in the  $(xy)$  plane. At each XUV photon energy, we scan the delay between the XUV pulse and the IR laser field ( $\tau$ ) in the range of 0 to 60 au in 7 increments.

### III. NUMERICAL RESULTS

We identify three regions in the photoelectron energies which display distinctively different PMD in the polarization plane. These regions can be characterized by the strength of the molecular two-center interference. The theory of this interference was proposed by Cohen and Fano [38] and Kaplan and Markin [39] and further developed for diatomic molecules fixed in space by Walter and Briggs [40]. In the latter formulation, the ionization amplitude is approximated by the expression

$$f_{\text{WB}}(\mathbf{k}) \propto (\mathbf{e} \cdot \mathbf{k}) \cos(\mathbf{k} \cdot \mathbf{R}/2), \quad (13)$$

where  $\mathbf{e}$  is the polarization vector of light and  $\mathbf{R}$  is the vector connecting the nuclei. The first term in the RHS of Eq. (13) is the atomic hydrogen dipole factor whereas the second term represents the molecular two-center interference. In the following, we will use a scalar coefficient  $c = kR/2$  to identify the strength of this interference.

#### A. Weak interference

At low photoelectron energy when  $c \ll 1$ , the PMD of H<sub>2</sub> looks essentially atomic like with very little anisotropy seen between the parallel and perpendicular orientation of the molecular axis  $\mathbf{R}$  relative to the linear polarization axis  $\mathbf{e}$  of the XUV pulse. This behavior is featured in Fig. 1 which displays the PMD at  $\Omega = 0.7$  au. The top and middle panels both illustrate the case of the parallel orientation with the XUV only pulse (top) and XUV+IR pulses (middle). The bottom panel displays the radially integrated PMD of the middle panel in the form of the

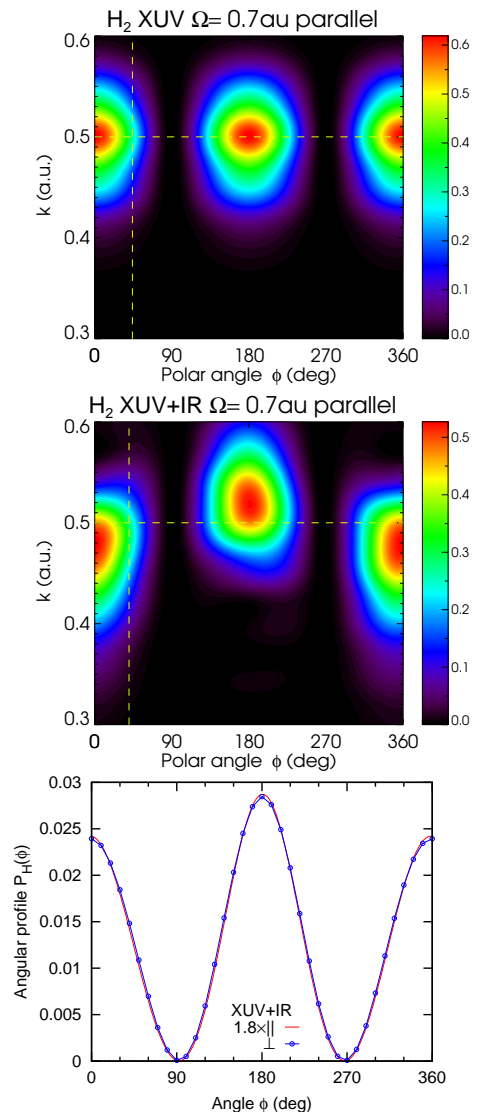


FIG. 1: Top: PMD of H<sub>2</sub> at  $\Omega = 0.7$  au in the parallel field orientation with the XUV only pulse (top) and the XUV+IR pulses (middle). The horizontal dashed line visualize the photoelectron momentum  $k_0 = \sqrt{2(\Omega - I_p)}$  from the energy conservation. The vertical dashed line mark the half of the angular width.

angular distribution  $P(\phi)$  which is overlapped with the analogous distribution for the perpendicular orientation. Except for an overall magnitude factor  $\times 1.8$ , the  $\perp$  angular distributions look essentially the same as the  $\parallel$  one.

Meanwhile, the PMD of the top panel (XUV only) and the middle panel (XUV+IR) differ by a noticeable displacement of the radial momentum by the vector-potential  $A_{\text{IR}}$  of the streaking field. To quantify this displacement, we use the central photoelectron momenta (12) in the downwards (-) and upwards (+) shifted lobes of the PMD

$$k_- \equiv \bar{k}(\phi = 0) \quad , \quad k_+ \equiv \bar{k}(\phi = \pi) \quad ,$$

These momenta  $k_{\pm}(\tau)$ , which depend sensitively on the XUV/IR time delay  $\tau$ , are then used to obtain the

isochrone phase offset:

$$k_{\pm}^2(\tau)/2 - E_0 = \pm A_0 k_{\pm}(\tau) \cos(\omega\tau + \Phi_S). \quad (14)$$

This determination is illustrated in the top panel of Fig. 2. Here we determine  $\Phi_S = -0.216 \pm 0.003$  rad by fitting either of the  $k_{\pm}(\tau)$  branches with a common streaking phase value over the whole set of the time delays  $\tau$ . Alternatively, we can apply Eq. (14) to individual  $\tau$  values and to determine the instantaneous  $\Phi_S(\tau)$ . These values are displayed along with the average streaking phase on the bottom panel of Fig. 2. Even though the variation of  $\Phi_S(\tau)$  exceeds the error bars of the average value, the accuracy of the instantaneous streaking phase determination is not significantly compromised.

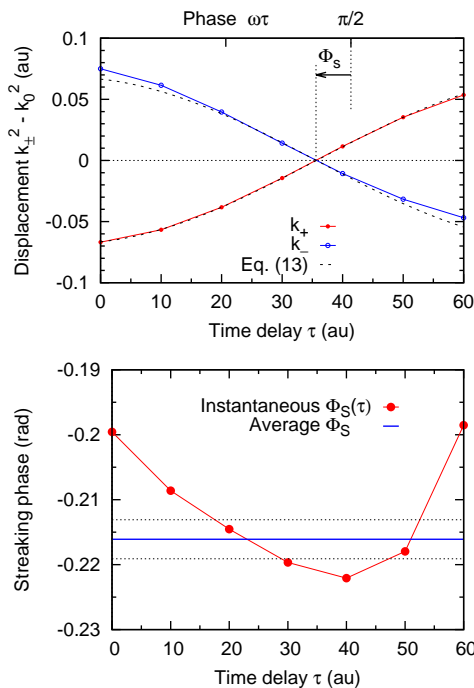


FIG. 2: Top: Radial momentum displacements  $k_{\pm}^2/2 - k_0^2/2$  are shown at various XUV/IR delays  $\tau$ . The dashed line represents the fit with Eq. (14). The arrow indicates the streaking phase  $\Phi_S$ . Bottom: the fit with Eq. (14) is applied to individual  $\tau$  values to determine the instantaneous  $\Phi_S(\tau)$ . The average  $\Phi_S$  is shown as a solid line with error bars visualized by dotted lines.

### B. Moderate interference

This region is characterized by a moderate factor  $c \lesssim 1$ . A typical PMD in this region is presented in the top and middle panels of Fig. 3. Here the XUV photon energy  $\Omega = 1.5$  au and the molecule is oriented parallel (top) and perpendicular (middle) to the polarization axis. Both panels visualize single-photon XUV ionization. Adding the IR streaking field does not change the PMD structure

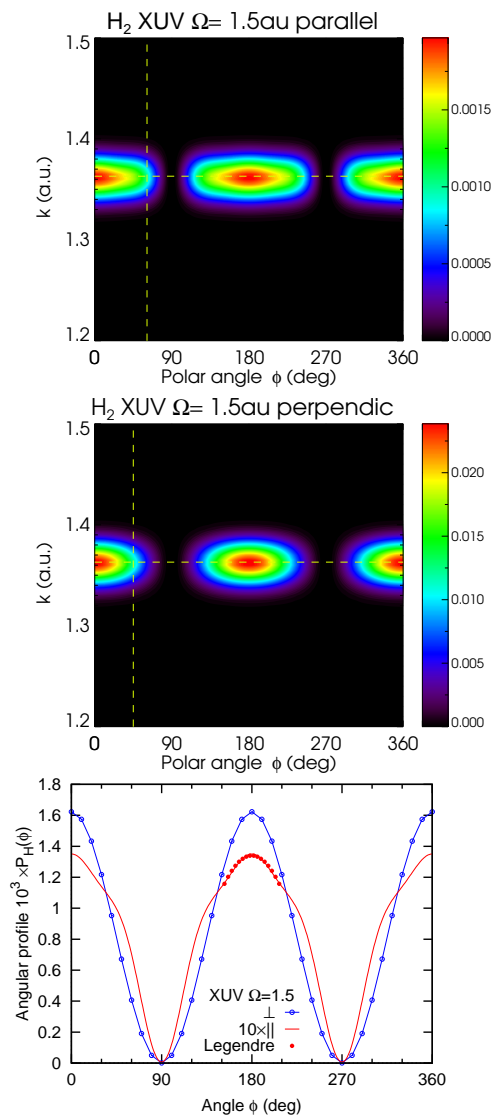


FIG. 3: Top: PMD of  $H_2$  at  $\Omega = 1.5$  au for the parallel (top) and perpendicular (middle) field orientation with the XUV only pulse. The horizontal dashed line visualizes the photoelectron momentum  $k_0$  while the vertical line marks half of the angular width.

except for a vertical up and down displacement by the amount of  $A_{IR}$  as in the middle panel of Fig. 1.

The case of  $c \lesssim 1$  differs from  $c \ll 1$  by a significant deviation of the PMD shapes corresponding to the parallel and perpendicular orientations. The PMD lobes are noticeably elongated for the parallel orientation and acquire a greater angular width. The photoelectron angular distribution shown in the bottom panel is markedly different for the  $\parallel$  and  $\perp$  orientations. While the latter retains the atomic like structure, the former widens significantly and becomes drastically, by a factor  $\times 10$ , suppressed. This parallel emission suppression is documented in the literature and termed the "confinement effect" [41, 42]. This corresponds to the dominant photoelectron  $p$ -wave trapped inside a one-dimensional box of length  $R$  when the momentum quantization condition  $kR = \pi$  satisfied

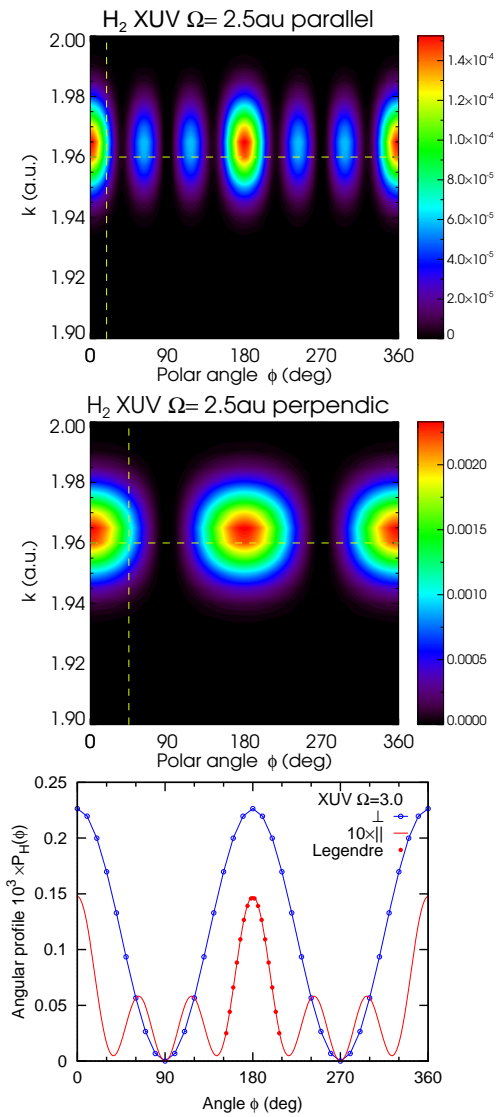


FIG. 4: Same as Fig. 3 for  $\Omega = 2.5$  au

at  $c = \pi/2$ .

### C. Strong interference

This region is characterized by a large interference factor  $c \gtrsim \pi/2$ . In this region, the shape distortion of PMD is most graphical as shown in Fig. 4 for  $\Omega = 2.5$  au. While the perpendicular orientation (middle panel) retains an atomic like shape, the parallel orientation (top panel) displays very clear interference fringes. These fringes are also seen in the angular resolved cross-section exhibited in the bottom panel of Fig. 4.

To quantify the two-center interference effects across a wide range of the photon energies, we plot in the bottom panel of Fig. 5 the half width of the PMD lobes. The atomic like half width of  $45^\circ$  corresponds to the dipole  $\cos^2 \phi$  angular shape. It is retained consistently over the whole photon energy range in the perpendicular molecular orientation for XUV only photoionization. Adding

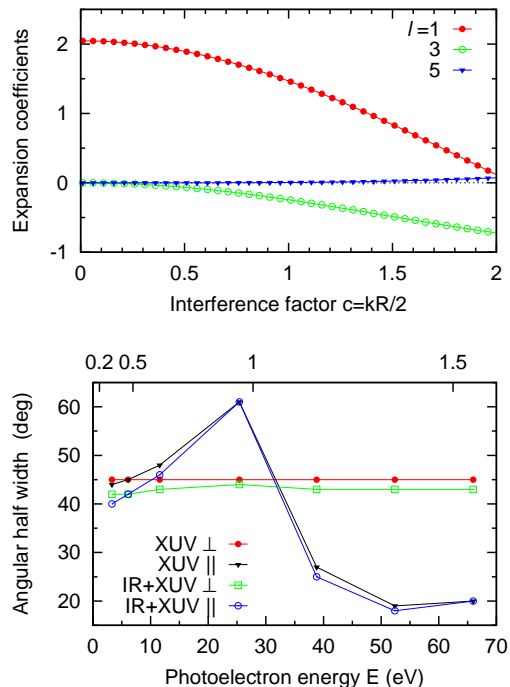


FIG. 5: Top: expansion coefficients of the ionization amplitude over the spherical harmonics (16) plotted as functions of the interference factor  $c = kR/2$ . Bottom: angular half width of the PMD lobes as a function of the photoelectron energy  $E = \Omega - I_p$ . The upper horizontal scale marks the corresponding interference factors.

a streaking IR field reduces this width insignificantly for the  $\perp$  orientation. Meanwhile, the  $\parallel$  orientation, both in XUV and XUV+IR fields, displays a wide oscillation of the width in the range of moderate to strong two-center interference.

To understand the nature of this oscillation, we note that the amplitude (13) for the parallel orientation is reduced to

$$f_{\text{WB}}^{\parallel}(\phi) \propto \cos \phi \cdot \cos(0.5kR \cos \phi). \quad (15)$$

This amplitude can be expanded over the spherical harmonics with the expansion coefficients given by the following expression [43]

$$A_{\ell}(c) = \langle Y_{\ell 0} | f_{\text{WB}}^{\parallel} \rangle = \sqrt{2\pi} \int_{-1}^1 \bar{P}_{\ell}(\eta) \eta \cos(c\eta) d\eta. \quad (16)$$

Here  $\bar{P}_{\ell}(\eta)$  are the normalized Legendre polynomials which depend on  $\eta = \cos \phi$ . The expansion coefficients (16) for various  $\ell$  are plotted in the top panel of Fig. 5. From this graph we see clearly that  $c \simeq 1$  corresponds to a noticeable contribution of the  $f$ -wave whereas at  $c \simeq \pi/2$  the  $p$ - and  $f$ -wave contributions become of the same magnitude. These two boundaries correspond to the region of moderate and strong two-center interference according to our classification in Sec. III B and Sec. III C. In the meantime, the weak interference  $c \ll 1$  considered in

Sec. III A corresponds to a nearly sole contribution of the  $p$ -wave.

Fitting the numerical TDSE results for the photoelectron angular distributions with the squared amplitude (15) gives systematically higher effective momenta  $k_{\text{eff}}$  in comparison with the nominal momenta  $k$  determined by the energy conservation. We find  $k_{\text{eff}}$  from the moduli ratio of the  $f$ - and  $p$ -waves

$$\left| \frac{A_3(c_a)}{A_1(c_a)} \right| = \left| \frac{\langle Y_{30} | f(\mathbf{k}) \rangle}{\langle Y_{10} | f(\mathbf{k}) \rangle} \right|. \quad (17)$$

This ratio equates the expansion coefficients  $A_\ell$  from Eq. (16) evaluated at  $c_a = k_{\text{eff}}R/2$  with the corresponding expansion coefficients of the exact numerical amplitude  $f(\mathbf{k})$  found by the TDSE solution.

The deviation  $k_{\text{eff}}$  from  $k$  displayed in the top panel of Fig. 6 can be explained by the effective potential of the ion remainder. Due to this potential, the momentum of the electron near the nucleus is greater, and, accordingly, a larger phase difference between the emitting centers is accumulated. We can introduce an average effective potential related to the effective momentum through the following expression

$$k_{\text{eff}}/k = \sqrt{1 + 2|\bar{U}_{\text{eff}}|/k^2}. \quad (18)$$

The values of  $\bar{U}_{\text{eff}}$  are presented in the bottom panel of Fig. 6. A gradual reduction of  $\bar{U}_{\text{eff}}$  with a decreasing XUV photon energy can be understood as follows. By the uncertainty principle, a slower photoelectron has a larger birthplace area across which the ionic potential is sampled. Therefore, its effective depth becomes smaller.

#### D. Streaking phase and time delay

The streaking phase results for the  $\text{H}_2$  molecule in the  $\parallel$  and  $\perp$  orientations are summarized in the top panel of Fig. 7 where they are compared with the corresponding values of the H atom. While the molecular  $\Phi_S$  in the  $\perp$  orientation is very similar to the atomic one, the  $\parallel$  orientation displays a systematically higher values, especially at the onset of the strong interference when the  $c$  factor approaching  $\pi/2$ . The atomic time delay derived from the streaking phase  $\tau_a = \Phi_S/\omega$  is shown in the bottom panel of Fig. 7 where it is compared with the corresponding values returned by the RABBITT simulations [32]. Numerical  $\tau_a$  values from the ASX and RABBITT simulations are slightly different because of a difference in the wavelength  $\lambda = 1200$  nm in the former and 800 nm in the latter. The IR photon wavelength and energy affect the CC component of the atomic time delay [29, 44] which becomes particularly noticeable close to the threshold. Nevertheless, the qualitative behavior of  $\tau_a$  is very similar in both sets of simulations. The atomic time delay in the H atom and the  $\text{H}_2$  molecule in the  $\perp$  orientation remain negative in the studied XUV photon energy range.

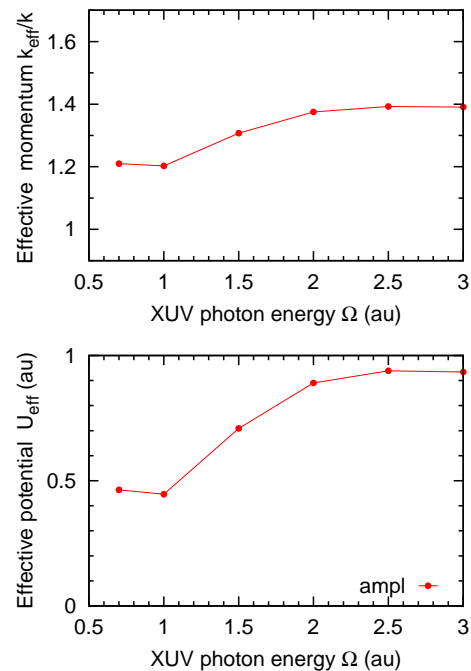


FIG. 6: Top: Effective momentum  $k_{\text{eff}}/k$ . Bottom: effective potential  $U_{\text{eff}}$ .

At the same time, the  $\parallel$  orientation displays a sharp rise of the time delay to positive values. This effect is also recorded in the  $\text{H}_2^+$  ion [33, 34]. It was attributed in [33] to the destructive two-center interference. We offer a more physically appealing interpretation of the positive time delay due to the trapping the photoelectron in the molecular potential well. From the condition of this trapping  $k_{\text{eff}}R = \pi$  occurring at  $kR \simeq 2.4$  we can estimate  $|U_{\text{eff}}| \simeq 1$  au. This determination is consistent with the values of  $U_{\text{eff}}$  presented in the bottom panel of Fig. 6.

## IV. CONCLUSIONS

In the present work, we employed the angular streaking of XUV ionization of the  $\text{H}_2$  molecule to determine the streaking phase and time delay corresponding to various orientations of the inter-nuclear axis relative to the polarization axis of ionizing radiation. The ASX technique was originally developed to characterize isolated attosecond pulses from XFEL source on the shot-to-shot basis. This technique was adapted to determine the streaking phase and applied in our previous work [31] to the atomic hydrogen. In the present work we expand this technique to diatomic homonuclear molecules. We converted the streaking phase to the atomic time delay and found it in good agreement with our earlier RABBITT simulations [32]. Unlike RABBITT, which requires an accurate and stable synchronization of the ionizing XUV and probing IR pulses, ASX can determine the streaking phase and time delay from a single XUV shot. This is essential in XFEL sources with their inherent time jitter.

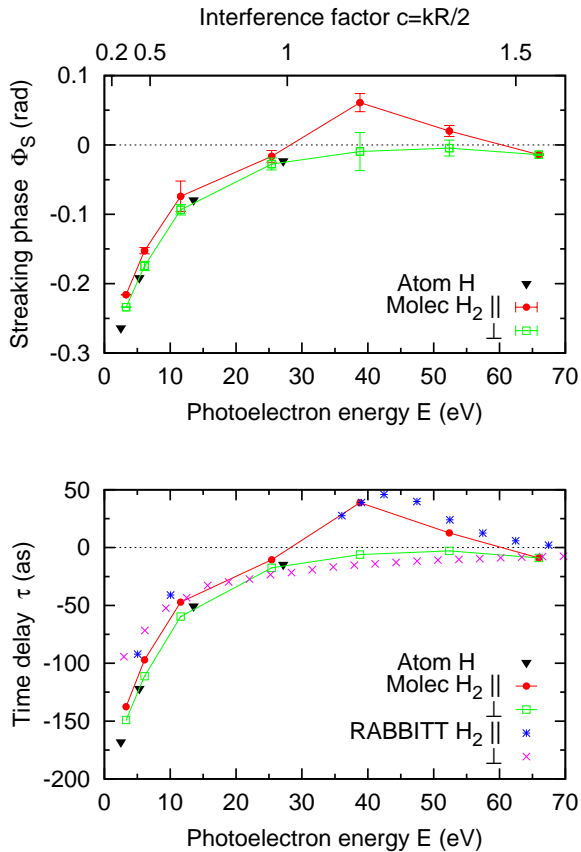


FIG. 7: Top: Streaking phase  $\Phi_S$  as a function of the photoelectron energy for the hydrogen atom and the  $H_2$  molecule in the  $\parallel$  and  $\perp$  orientations. Bottom: the atomic time delay derived from the streaking phase  $\tau_a = \Phi_S/\omega$  is compared with the corresponding values returned from the RABBITT simulations [32].

As in earlier works [32–34] we observe a strong orientation dependence of the molecular time delay. In most cases,  $\tau_a$  remains negative in H,  $H_2$  and  $H_2^+$  due to a large negative CC component. However,  $\tau_a$  becomes positive in  $H_2$  and  $H_2^+$  in the parallel orientation  $\mathbf{R} \parallel \mathbf{e}$ . This happens when the photoelectron in the dominant  $p$ -wave becomes trapped in the molecular potential well. From the condition of this trapping we can estimate the depth of this well  $U_{\text{eff}}$ .

While the streaking phase retrieval by ASX was demonstrated for a diatomic homo-nuclear molecule  $H_2$ , the proposed method should work for arbitrary molecular targets. Its application in XFEL will be particularly beneficial for studying inner shell ionization in atomic and molecular targets which cannot be ionized at present with conventional laser HHG sources.

*Acknowledgment:* We thank Rickson Wielian for reviewing the literature and useful discussions. This work is supported by the Discovery grant DP190101145 of the Australian Research Council. Resources of National Computational Infrastructure facility (NCI Australia) have been employed.

- 
- [1] M. Huppert, I. Jordan, D. Baykusheva, A. von Conta, and H. J. Wörner, *Attosecond delays in molecular photoionization*, Phys. Rev. Lett. **117**, 093001 (2016).
- [2] H. Müller, *Reconstruction of attosecond harmonic beating by interference of two-photon transitions*, Appl. Phys. B **74**, s17 (2002).
- [3] E. S. Toma and H. G. Müller, *Calculation of matrix elements for mixed extreme-ultraviolet-infrared two-photon above-threshold ionization of argon*, J. Phys. B **35**(16), 3435 (2002).
- [4] L. Cattaneo, J. Vos, R. Y. Bello, A. Palacios, S. Heuser, L. Pedrelli, M. Lucchini, C. Cirelli, F. Martín, and U. Keller, *Attosecond coupled electron and nuclear dynamics in dissociative ionization of  $H_2$* , Nature Physics **14**, 733 (2018).
- [5] J. Vos, L. Cattaneo, S. Patchkovskii, T. Zimmermann, C. Cirelli, M. Lucchini, A. Kheifets, A. S. Landsman, and U. Keller, *Orientation-dependent stereo Wigner time delay in a small molecule*, Science **360**(6395), 1326 (2018).
- [6] S. Nandi, E. Plésiat, S. Zhong, A. Palacios, D. Busto, M. Isinger, L. Neoricic, C. L. Arnold, R. J. Squibb, R. Feifel, et al., *Attosecond timing of electron emission from a molecular shape resonance*, Science Advances **6**(31), eaba7762 (2020).
- [7] A. Kamalov, A. L. Wang, P. H. Bucksbaum, D. J. Haxton, and J. P. Cryan, *Electron correlation effects in attosecond photoionization of  $CO_2$* , Phys. Rev. A **102**, 023118 (2020).
- [8] A. L. Wang, V. V. Serov, A. Kamalov, P. H. Bucksbaum, A. Kheifets, and J. P. Cryan, *Role of nuclear-electronic coupling in attosecond photoionization of  $H_2$* , Phys. Rev. A **104**, 063119 (2021).
- [9] L. Young, K. Ueda, M. Gühr, P. H. Bucksbaum, M. Simon, S. Mukamel, N. Rohringer, K. C. Prince, C. Masciovecchio, M. Meyer, et al., *Roadmap of ultrafast x-ray atomic and molecular physics*, J. Phys. B **51**(3), 032003 (2018).
- [10] N. Hartmann, G. Hartmann, R. Heider, M. S. Wagner, M. Ilchen, J. Buck, A. O. Lindahl, C. Benko, J. Grünert, J. Krzywinski, et al., *Attosecond time-energy structure of x-ray free-electron laser pulses*, Nature Photonics **12**, 215 (2018).
- [11] J. Duris, S. Li, T. Driver, E. G. Champenois, J. P. MacArthur, A. A. Lutman, Z. Zhang, P. Rosenberger, J. W. Aldrich, R. Coffee, et al., *Tunable isolated attosecond x-ray pulses with gigawatt peak power from a free-*

- electron laser*, Nature Photonics **14**, 30 (2020).
- [12] Z. X. Zhao, Z. Chang, X. M. Tong, and C. D. Lin, *Circularly-polarized laser-assisted photoionization spectra of argon for attosecond pulse measurements*, Opt. Express **13**(6), 1966 (2005).
- [13] A. K. Kazansky, A. V. Bozhevolnov, I. P. Sazhina, and N. M. Kabachnik, *Interference effects in angular streaking with a rotating terahertz field*, Phys. Rev. A **93**, 013407 (2016).
- [14] S. Li, Z. Guo, R. N. Coffee, K. Hegazy, Z. Huang, A. Natan, T. Osipov, D. Ray, A. Marinelli, and J. P. Cryan, *Characterizing isolated attosecond pulses with angular streaking*, Opt. Express **26**(4), 4531 (2018).
- [15] A. K. Kazansky, I. P. Sazhina, and N. M. Kabachnik, *Fast retrieval of temporal characteristics of fel pulses using streaking by thz field*, Opt. Express **27**(9), 12939 (2019).
- [16] P. Eckle, M. Smolarski, P. Schlup, J. Biegert, A. Staudte, M. Schoffler, H. G. Muller, R. Dorner, and U. Keller, *Attosecond angular streaking*, Nat. Phys. **4**, 565 (2008).
- [17] P. Eckle, M. Smolarski, P. Schlup, J. Biegert, A. Staudte, M. Schoffler, H. G. Muller, R. Dorner, and U. Keller, *Attosecond angular streaking*, Nat Phys **4**, 565 (2008).
- [18] A. N. Pfeiffer, C. Cirelli, M. Smolarski, D. Dimitrovski, M. Abu-samha, L. B. Madsen, and U. Keller, *Attoclock reveals natural coordinates of the laser-induced tunnelling current flow in atoms*, Nat Phys **8**, 76 (2012).
- [19] E. Constant, V. D. Taranukhin, A. Stolow, and P. B. Corkum, *Methods for the measurement of the duration of high-harmonic pulses*, Phys. Rev. A **56**, 3870 (1997).
- [20] J. Itatani, F. Quéré, G. L. Yudin, M. Y. Ivanov, F. Krausz, and P. B. Corkum, *Attosecond streak camera*, Phys. Rev. Lett. **88**, 173903 (2002).
- [21] E. Goulielmakis, M. Uiberacker, R. Kienberger, A. Baltuska, V. Yakovlev, A. Scrinzi, T. Westerwalbesloh, U. Kleineberg, U. Heinzmann, M. Drescher, et al., *Direct measurement of light waves*, Science **305**(5688), 1267 (2004).
- [22] R. Kienberger, E. Goulielmakis, M. Uiberacker, A. Baltuska, V. Yakovlev, F. Bammer, A. Scrinzi, T. Westerwalbesloh, U. Kleineberg, U. Heinzmann, et al., *Atomic transient recorder*, Nature **427**, 817 (2004).
- [23] V. S. Yakovlev, F. Bammer, and A. Scrinzi, *Attosecond streaking measurements*, J. Mod. Opt. **52**(2-3), 395 (2005).
- [24] U. Frühling, M. Wieland, M. Gensch, T. Gebert, B. Schütte, M. Krikunova, R. Kalms, F. Budzyn, O. Grimm, J. Rossbach, et al., *Single-shot terahertz-field-driven x-ray streak camera*, Nature Photonics **3**, 523 (2009).
- [25] C.-H. Zhang and U. Thumm, *Streaking and Wigner time delays in photoemission from atoms and surfaces*, Phys. Rev. A **84**, 033401 (2011).
- [26] M. Ivanov and O. Smirnova, *How accurate is the attosecond streak camera?*, Phys. Rev. Lett. **107**, 213605 (2011).
- [27] X. Zhao, S. Li, T. Driver, V.-H. Hoang, A.-T. Le, J. P. Cryan, A. Marinelli, and C. D. Lin, *Characterization of single-shot attosecond pulses with angular streaking photoelectron spectra*, Phys. Rev. A **105**, 013111 (2022).
- [28] J. M. Dahlström, A. L. Huillier, and A. Maquet, *Introduction to attosecond delays in photoionization*, J. Phys. B **45**(18), 183001 (2012).
- [29] J. M. Dahlström *et al*, *Theory of attosecond delays in laser-assisted photoionization*, Chem. Phys. **414**, 53 (2013).
- [30] A. Maquet, J. Caillat, and R. Taïeb, *Attosecond delays in photoionization: time and quantum mechanics*, J. Phys. B **47**(20), 204004 (2014).
- [31] A. S. Kheifets, R. Wielian, I. A. Ivanov, A. L. Wang, A. Marinelli, and J. P. Cryan, *Phase retrieval from angular streaking of XUV atomic ionization (2022)*, URL <https://arxiv.org/abs/2202.06147>.
- [32] V. V. Serov and A. S. Kheifets, *Time delay in XUV/IR photoionization of H<sub>2</sub>O*, J. Chem. Phys. **147**(20), 204303 (2017).
- [33] Q.-C. Ning, L.-Y. Peng, S.-N. Song, W.-C. Jiang, S. Nagele, R. Pazourek, J. Burgdörfer, and Q. Gong, *Attosecond streaking of Cohen-Fano interferences in the photoionization of H<sub>2</sub><sup>+</sup>*, Phys. Rev. A **90**, 013423 (2014).
- [34] V. V. Serov and A. S. Kheifets, *Angular anisotropy of time delay in XUV+IR photoionization of H<sub>2</sub><sup>+</sup>*, Phys. Rev. A **93**, 063417 (2016).
- [35] M. Kitzler, N. Milosevic, A. Scrinzi, F. Krausz, and T. Brabec, *Quantum theory of attosecond XUV pulse measurement by laser dressed photoionization*, Phys. Rev. Lett. **88**, 173904 (2002).
- [36] M. Schultze, M. Fiess, N. Karpowicz, J. Gagnon, M. Korbman, M. Hofstetter, S. Neppl, A. L. Cavalieri, Y. Komninos, T. Mercouris, et al., *Delay in Photoemission*, Science **328**(5986), 1658 (2010).
- [37] V. V. Serov, *Calculation of intermediate-energy electron-impact ionization of molecular hydrogen and nitrogen using the paraxial approximation*, Phys. Rev. A **84**, 062701 (2011).
- [38] H. D. Cohen and U. Fano, *Interference in the photoionization of molecules*, Phys. Rev. **150**, 30 (1966).
- [39] I. G. Kaplan and A. P. Markin, *Interference phenomena in photoionization of molecules*, Sov. Phys. Dokl. **14**, 36 (1969).
- [40] M. Walter and J. Briggs, *Photo-double ionization of molecular hydrogen*, J. Phys. B **32**(11), 2487 (1999).
- [41] J. Fernández, O. Fojón, A. Palacios, and F. Martín, *Interferences from fast electron emission in molecular photoionization*, Phys. Rev. Lett. **98**, 043005 (2007).
- [42] J. Fernández, F. L. Yip, T. N. Rescigno, C. W. McCurdy, and F. Martín, *Two-center effects in one-photon single ionization of H<sub>2</sub><sup>+</sup>, H<sub>2</sub>, and Li<sub>2</sub><sup>+</sup> with circularly polarized light*, Phys. Rev. A **79**, 043409 (2009).
- [43] V. V. Serov, I. A. Ivanov, and A. S. Kheifets, *Single-photon double ionization of H<sub>2</sub> away from equilibrium: A showcase of two-center electron interference*, Phys. Rev. A **86**, 025401 (2012).
- [44] V. V. Serov, V. L. Derbov, and T. A. Sergeeva, *Interpretation of the Time Delay in the Ionization of Coulomb Systems by Attosecond Laser Pulses*, *Advanced Lasers: Laser Physics and Technology for Applied and Fundamental Science* (Springer Netherlands, Dordrecht, 2015), pp. 213–230, ISBN 978-94-017-9481-7.